Available online at www.sciencedirect.com
SCIENCE DIRECT®
Journal of Solid State Chemistry 174 (2003) 257–263
JOURNAL OF SOLID STATE CHEMISTRY
http://elsevier.com/locate/jssc

Enhanced ferromagnetic transition and magnetoresistance in granular Ag-added $La_{0.7}Ca_{0.3}MnO_3$

Yun-Hui Huang,[a,1] Ke-Feng Huang,[a] Feng Luo,[a] Lian-Long He,[b] Zhe-Ming Wang,[a] Chun-Sheng Liao,[a] and Chun-Hua Yan[a,*]

[a] *State Key Lab of Rare Earth Materials Chemistry and Applications and PKU-HKU Joint Lab in Rare Earth Materials and Bioinorganic Chemistry, College of Chemistry and Molecular Engineering, Peking University, Beijing 100871, China*

[b] *Shenyang National Laboratory for Materials Science, Institute of Metal Research, Chinese Academy of Sciences, Shenyang 110016, China*

Received 30 January 2003; received in revised form 7 April 2003; accepted 9 April 2003

Abstract

Granular Ag-added $La_{0.7}Ca_{0.3}MnO_3$ (LCMO) samples were prepared by a sol–gel chemical route. Significant enhancements in Curie temperature (T_C), metal−insulator transition (T_p) and magnetoresistance (MR) effects near room temperature are observed in as-obtained samples. 10 wt% addition of Ag in LCMO causes T_C shift from 272 to 290 K, T_p boost up for more than 100 K and resistivity decrease by more than 3 orders of magnitude. X-ray diffraction patterns, thermal analysis and energy dispersive analysis of X-rays evidently show the existence of metal silver in LCMO matrices. High-resolution electron microscopy illustrates a well crystallization for LCMO grains in existence of Ag. It is argued that improved grain boundary effect and better crystallization caused by Ag addition are responsible for the enhancements.

Keywords: Ag-added $La_{0.7}Ca_{0.3}MnO_3$; Synthesis; Magnetic behavior; Transport

1. Introduction

Large numbers of studies have shown that Curie temperature (T_C) and metal−insulator (M−I) transition temperature (T_p) for doped manganites $La_{1-x}Ca_xMnO_3$ are strongly dependent on the composition and microstructure [1–5]. Based on the double-exchange model, the magnetic and electrical properties are explained by considering the magnetic coupling between neighboring Mn^{3+} and Mn^{4+} ions [6]. Thus, the Mn^{4+} content is the crucial parameter for determining the observed T_C and T_p. In addition, preparation condition can also modify the magnetic and transport properties due to its influence on microstructure. It has been reported that the samples with special microstructure fabricated through special processing would achieve anomalous behaviors, such as enhanced T_C and T_p [7–9]. By improving the preparation route or achieving inhomogeneous composition, it is possible for the La–Ca based manganites to obtain ferromagnetic and M−I transitions at temperatures higher than predicted by the commonly accepted phase diagram [2]. This is meaningful for physics and practical applications.

Very recently, Ag-doped lanthanum manganite films have inspired much interest due to observations of enhanced T_C, T_p or temperature coefficient of resistance [10–13]. In our previous paper [14], we found an enhanced magnetoresistance (MR) near room temperature and a reduced resistivity dependent on calcination temperature above or below the melting point of Ag in $La_{0.7}Ca_{0.3}MnO_3$/Ag two-phase composites. Thus, Ag addition has a special contribution in the magnetic and transport properties of the manganites.

As we have known, considerable wide-temperature-range MR and low-field MR originated from spin-polarized electron tunneling are observed in the polycrystalline manganites [15,16], but the existence of grain boundaries (GBs) leads to a downshift of M−I transition and an increase of resistivity. In this paper, we

*Corresponding author. Fax: +86-10-62754179.
E-mail address: chyan@chem.pku.edu.cn (C.-H. Yan).
[1] Present address: Institute of Advanced Materials and Technology, Fudan University, Shanghai, China.

0022-4596/03/$ - see front matter © 2003 Elsevier Inc. All rights reserved.
doi:10.1016/S0022-4596(03)00212-3

try to insert metal Ag into manganite matrices to modify GBs, leading to the improvement of the properties. Granular $La_{0.7}Ca_{0.3}MnO_3$ (LCMO) was prepared by a sol–gel chemical route in existence of $AgNO_3$. Metal silver was synchronously formed in the same system. Significant enhancements in T_C and T_p, dramatic reduction in resistivity, and also an improved MR near room temperature are observed. The calcination behavior, morphology, and the influence of Ag content on magnetic/transport behaviors are investigated.

2. Experimental

We express the Ag-added $La_{0.7}Ca_{0.3}MnO_3$ as $(LCMO)_{1-x}Ag_x$ (x is nominal weight fraction of Ag). The samples were prepared by the method based on thermal decomposition of precursor complexes through one step. $AgNO_3$ served as the source of Ag. Stoichiometric nitrates of La^{3+}, Ca^{2+}, and Mn^{2+}, the starting chemicals for preparation of LCMO, were dissolved in distilled water. Ethylenediaminetetraacetic acid (EDTA), a complexant, was added as its ammonium salt to form La–Ca–Mn precursor solution, in which the molar ratio of total metal ions to EDTA was 1:1.5. With continuously stirring, $AgNO_3$ aqueous solution in calculated weight ratio was then added dropwise to achieve a transparent uniform precursor solution with $pH \approx 9$ adjusted with ammonia. By considering the complexing constants, Ag^+ is formed to be $Ag(NH_3)_2^+$, whereas La^{3+}, Sr^{2+} and Mn^{2+} exist as their corresponding complexes with EDTA in such a solution that favors the formation of segregate LCMO and silver phases in the final samples. Then the solution was evaporated in a porcelain crucible at about 110°C to yield an amorphous gel, and subsequently, the gel ignited spontaneously to turn into a raw ash when excess free water evaporated. The as-prepared ash was pressed into pellets with diameter of 6 mm and finally calcined at 800°C for 2 h in a stagnant air to obtain the target samples.

The phases were determined by an X-ray diffraction (XRD, D/max-2000, Cu$K\alpha$, Rigaku). The micrograph was probed by scanning electronic microscope (SEM, Amary, FE-1910), and high-resolution transmission electron microscopy (HRTEM) observations were performed using a JEM-2010 electron microscope. The compositions were examined by energy dispersive analysis of X-rays (EDX) in SEM. Thermal calcination behavior was obtained by a DuPont 2100 thermal analyzer. Magnetic and transport measurement was performed on a MagLab System 2000 (Oxford, UK). Resistance was obtained using a standard four-probe technique at temperature from 5 to 300 K.

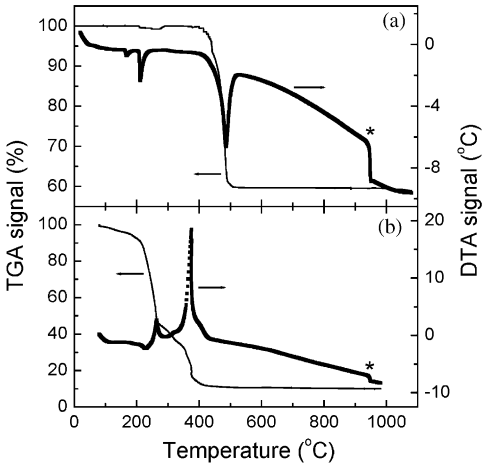

Fig. 1. Combined TGA–DTA runs for (a) $AgNO_3$ and (b) precursor xerogel of $(LCMO)_{0.9}Ag_{0.1}$. The labeled asterisks represent the melting point of Ag.

3. Results and discussion

First, calcination behaviors for $AgNO_3$ and precursor xerogel of $(LCMO)_{0.9}Ag_{0.1}$ are investigated. Fig. 1 shows their combined thermogravimetric analysis (TGA)–differential thermal analysis (DTA) runs. For $AgNO_3$, a continuous weight loss occurs from 420°C to 500°C, accompanied by an endothermic heat effect at 480°C. This loss exactly accords with the decomposition process from $AgNO_3$ to Ag_2O and subsequently to metal Ag. From 500°C to 900°C, only little weight loss is observed, and no thermal effect occurs, showing that the metal silver is stable within this temperature range. A second weight loss as well as an endothermic DTA signal appears at 950°C, which is caused by melting of Ag. Thus the melting temperature (T_m) of Ag is around 950°C. For the precursor xerogel, three weight losses and a large exothermic peak centering at 380°C corresponding to the formation of LCMO are clearly observed [17]. The weight loss and thermal effect related to Ag are overlapped by those of LCMO before 500°C, but still appear at around 950°C. In our experiment, the final calcination temperature of 800°C not only favors the formation of both LCMO and metal silver, but also avoids the melting of Ag.

Because of the existence of metal Ag in the samples, it is difficult to determine the content of every element through wet chemical routes. We use EDX analysis in SEM to qualitatively check the composition. EDX results show the same composition of La, Ca and Mn as the expected LCMO within error limits of the measurement, but the detected Ag content x is much lower than the nominal one due to volatilization of Ag during calcinations (see Table 1). The larger the nominal x, the larger weight loss for silver. Because the values of detected x for the samples with nominal $x = 0.15$ and

Table 1
Characterizations of $(LCMO)_{1-x}Ag_x$ samples

Nominal x	0	0.02	0.05	0.10	0.15	0.20
x obtained by EDX	0	0.016	0.018	0.035	0.039	0.047
LCMO grain size D (nm)	28.7	26.2	26.2	29.6	28.5	26.4
Lattice constant a (Å)	3.8687	3.8621	3.8583	3.8622	3.8587	3.8610

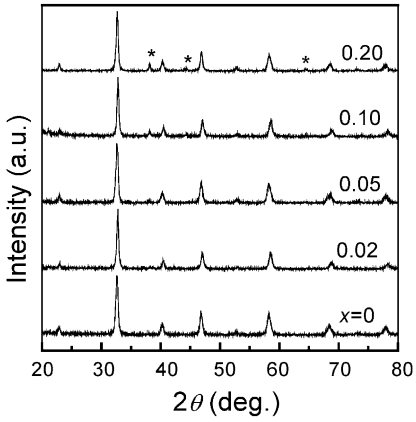

Fig. 2. X-ray diffraction patterns for $(LCMO)_{1-x}Ag_x$ samples with $x = 0$, 0.02, 0.05, 0.10 and 0.20. The asterisks represent the peaks caused by metal silver.

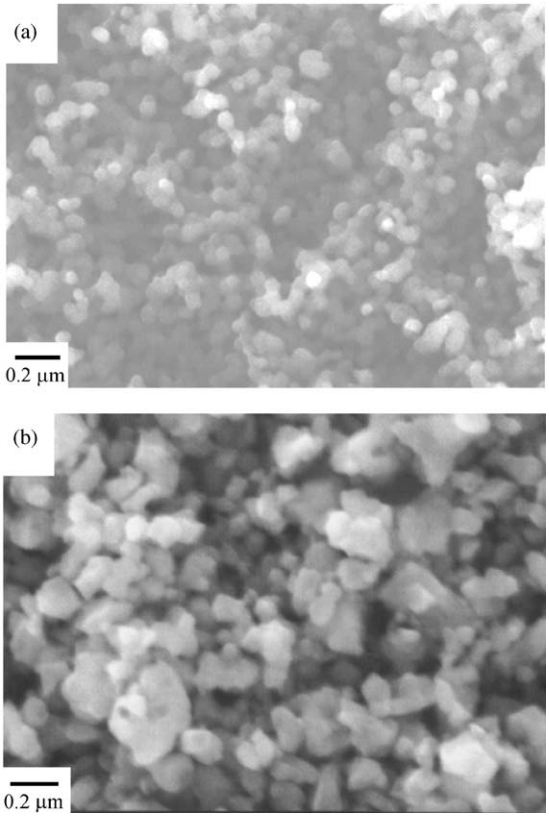

Fig. 3. Cross-sectional SEM micrographs for (a) LCMO and (b) typical $(LCMO)_{0.9}Ag_{0.1}$.

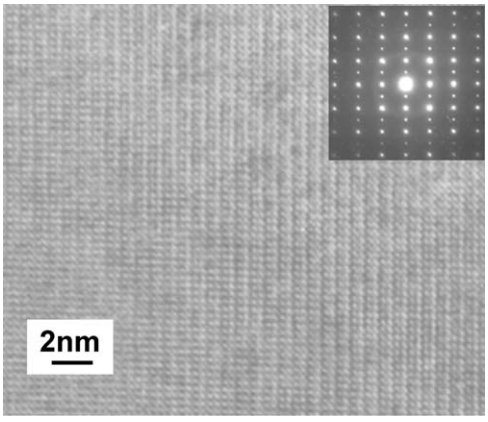

Fig. 4. Typical HRTEM image along the [001] direction of a single LCMO grain in $(LCMO)_{0.9}Ag_{0.1}$; the inset shows the corresponding SAED pattern.

0.20 are very close to that of $x = 0.10$, we only investigate the magnetic and transport properties for the samples with the nominal x varying from 0 up to 0.10. Fig. 2 displays the XRD patterns of $(LCMO)_{1-x}Ag_x$ samples with different Ag content. LCMO is of single phase indexed by cubic lattice symmetry. For the composites, the diffraction peaks centered at $2\theta = 38.1°$ (111), 44.3° (200) and 64.4° (220) caused by cubic Ag can be clearly observed, as labeled by the asterisks, and the intensity increases with x. This strongly confirms the presence of metal silver. From the XRD peaks, the average grain size (D) can be calculated using the Scherrer formula: $D = 0.9\lambda/\beta\cos\theta$, where λ is the X-ray wavelength employed, θ is the diffraction angle of the most intense peak (110), and β is defined as $\beta^2 = \beta_m^2 - \beta_s^2$, β_m and β_s are the experimental full-width at half-maximum (FWHM) and the FWHM of a standard silicon sample. The as-obtained D of silver is around 50 nm. The D of LCMO grains varies within 26 and 29 nm, which is almost independent of Ag content, as shown in Table 1. Therefore, LCMO grains do not grow up in spite of the existence of silver.

Fig. 3 shows the SEM images for typical $(LCMO)_{1-x}Ag_x$ samples with $x = 0$ and 0.10. It is difficult for us to distinguish the two phases of Ag and LCMO owing to their approximate sizes. However, compared to the sample without Ag, LCMO crystallites in Ag-added sample are more perfect and homogeneous. We display a typical HRTEM image of a single LCMO grain of $(LCMO)_{0.9}Ag_{0.1}$ in Fig. 4. A regular contrast is observed, which mainly consists of a square array of bright spots, spaced by about 2.8 Å. The image fits well with the simulated one for the cubic structure. This cubic structure can be further confirmed by the selected area electron diffraction pattern (SAED) in the inset.

We can also demonstrate the discrepancy in crystallization by structural changes. The structural changes can well reflect the variations in oxygen content and hence the Ag-caused oxygenation effect. As displayed in Table 1, the lattice axis parameter a for LCMO is 3.8687 Å. A small decrease in a related with the increase in oxygen content is found in Ag-added samples. Obviously, Ag helps in better oxygenation of LCMO, which is attributed to the release of atomic oxygen during the decomposition of $AgNO_3$. This is the important reason for the improvement of morphology.

Thermal magnetization curves for $x = 0$, 0.05 and 0.10 are presented in Fig. 5. The pure LCMO undergoes a broad ferro/paramagnetic (FM/PM) transition due to boundary effects in the small-grain systems [17], whereas the magnetic transition becomes sharper with addition of Ag. The Curie temperature T_C, obtained by the minimum dM/dT, is 272 K for LCMO, in agreement with the reported maximal value for LCMO series [18]. T_C remarkably upshifts toward room temperature, e.g., T_C is 280 K for $x = 0.05$ and 290 K for $x = 0.10$. 10 wt% addition of Ag enhances T_C by 18 K. In addition, the magnetization M is greatly enhanced by Ag addition. The inset of Fig. 5 shows the M as a function of applied magnetic field for typical samples with $x = 0$ and 0.10. Both of the two samples possess long-range ferromagnetic order at low temperature. It is surprising that the inclusion of nonmagnetic Ag significantly enhances the magnetization. The results of T_C and M can be well reproducible by the parallel samples on superconducting quantum interference device (SQUID) magnetometer. When Ag is introduced into the manganite, it can be doped into La-site to enhance the Mn^{4+} content. In our preparation condition, Ag^+ is difficult to enter the La-site due to the unfavorable competition with Ca^{2+}, low calcination temperature and short calcination time. Although it was found that the single-phase polycrystalline $La_{1-x}Ag_xMnO_3$ could be formed without existence of Ca^{2+}, the T_C is only 215 and 240 K for $x = 0.05$ and 0.10, respectively, much lower than the T_C observed in our case [19]. Obviously, the present enhancement of T_C and M is impossibly caused by substitution of Ag^+ for La^{3+}. We suggest that well crystallization and uniform of LCMO grains induced by Ag are the main reasons of this enhancement. In general, for granular LCMO, the grain boundary effect is striking, which means that the magnetic configuration at the grain surfaces or boundaries is much chaotic, giving rise to a weak coupling among the magnetic ions. With the addition of Ag, crystallization and homogeneity of LCMO are improved; as a consequence, magnetic scattering at GBs is suppressed.

Similar enhancement is also found in the M–I transition. Fig. 6 presents the zero-field resistivity (ρ) as a function of temperature for $x = 0$, 0.02, 0.05 and 0.10. The transition temperature T_p of $x = 0$ is 105 K, which is much lower than the corresponding T_C. Notably, the T_p is 212, 228 and 250 K for $x = 0.02$, 0.05 and 0.10, all of which are enhanced by more than 100 K than that of LCMO. For $x = 0.10$, a sharp drop in ρ appears at about 270 K where the intrinsic M–I transition occurs. It is well known that the single crystals, epitaxial thin films and ceramic bulk samples of the manganites can exhibit intrinsic behaviors, which T_p's commonly appear in the vicinity of the corresponding T_C's. However, for the granular manganites, imperfect crystallization in GBs causes the existence of intergrain insulating regions due to the bad connectivity between grains, and consequently leads to the lower T_p [20,21]. In the present Ag-added samples, Ag grains are dispersed into LCMO matrices as confirmed by XRD

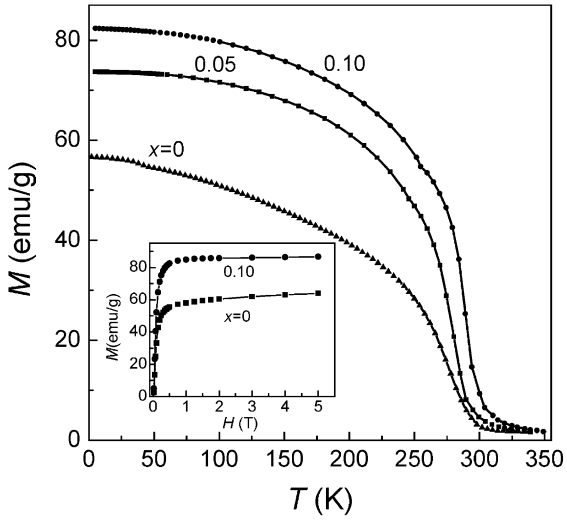

Fig. 5. Magnetization M as a function of temperature for $(LCMO)_{1-x}Ag_x$ with $x = 0$, 0.05 and 0.10 under an applied field of 0.5 T; the inset shows the field dependence of M at 5 K.

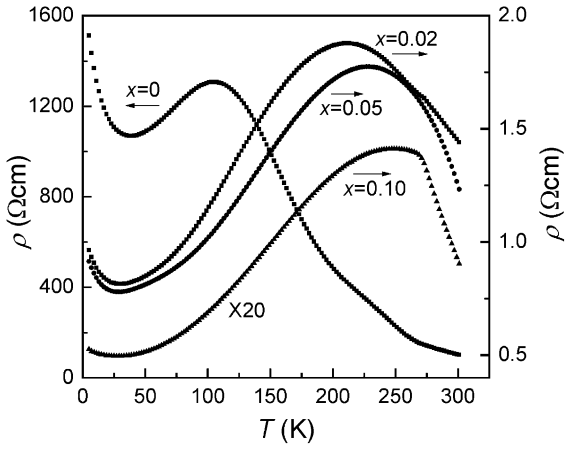

Fig. 6. Temperature dependence of zero-field resistivity (ρ) for $(LCMO)_{1-x}Ag_x$.

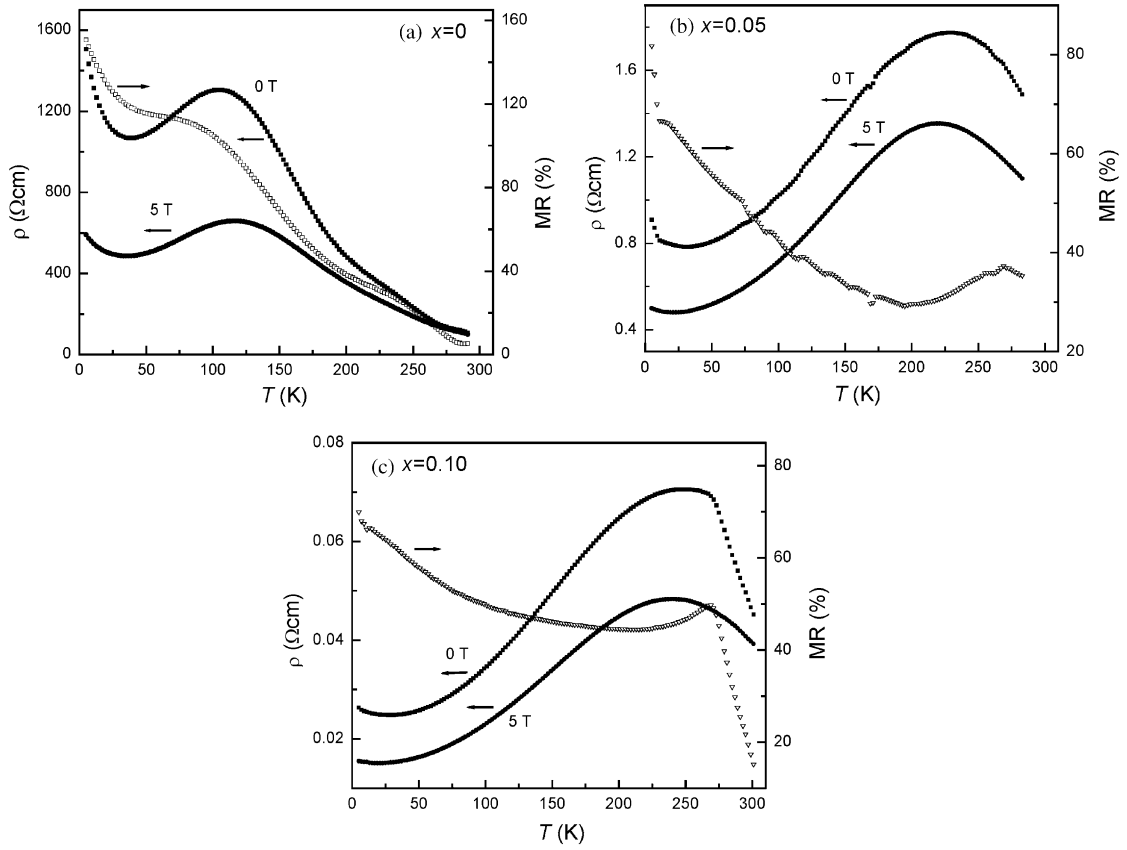

Fig. 7. Temperature dependence of resistivity (ρ) at 0 and 5 T, and MR ratio for $(LCMO)_{1-x}Ag_x$.

patterns. The variation in T_p caused by Ag can be well understood by the transport model of parallel connected conduction channels proposed by Andrés et al. [20]. The existence of metal silver opens a new conduction channel blocked at GBs, which is responsible for the T_p enhancement. The extent of this enhancement depends on the proportion of the metallic conduction in the sample. Meanwhile, the metallic conduction can also give rise to the decrease in ρ. We can observe that the magnitude of ρ is lowered by 3 or more orders of magnitude due to Ag addition. It is notable that ρ is dramatically reduced to near $10^{-2}\,\Omega$ cm when $x = 0.10$, which can be comparative to that of ceramic or single-crystal LCMO. For granular systems, it is well established that the transport is mainly controlled by the spin-polarized tunneling [14]. The insulating regions in GBs can be served as tunnel barriers. The low-temperature resistivity in Fig. 6 can provide further evidence for Ag influence on GBs. As we have seen, an upturn of resistivity occurs at 38, 32, 29 and 30 K for $x = 0$, 0.02, 0.05 and 0.10, respectively. This upturn is due to the existence of an intergranular Coulomb gap, which adds to the tunnel barriers [22]. It is clear that Ag addition leads to a decrease in the upturn temperature, indicative of suppression of the extrinsic behaviors. Therefore, the decrease in the upturn temperature is in agreement with the enhancement in T_p from the viewpoint of GBs.

Fig. 7 shows temperature dependence of resistivity and MR ratio (defined as $(\rho_0 - \rho_H)/\rho_H$) for $(LCMO)_{1-x}Ag_x$ with different Ag content. Because of the small grain sizes, MR effect only occurs at low temperatures and collapses at high temperatures for pure LCMO. However, although LCMO grains do not grow up, the Ag-added samples exhibit significant enhanced MR effect at high temperatures. For $x = 0.10$, the sample possesses a MR peak near T_C. Another interesting behavior is the abnormal magnetic-field dependence of T_p in the Ag-added samples. As shown in Figs. 7(b) and (c), T_p decreases with increasing magnetic field, which is opposite from the common observation for LCMO in Fig. 7(a). In fact, application of a magnetic field will give the field-induced FM ordering and hence lead to the reduced resistivity and shifting of T_p to a higher temperature. Ag-added samples are very complicated in physical nature. In our opinion, the abnormal field induced may be attributed to coexistence of extrinsic and intrinsic transport behaviors. The peak of resistivity at an applied field does not reflect the real M–I transition, but reflect

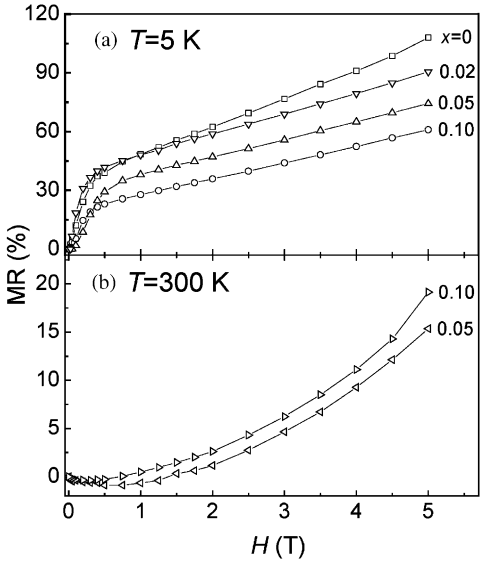

Fig. 8. MR ratio as a function of applied field for $(LCMO)_{1-x}Ag_x$: (a) at 5 K and (b) at 300 K.

the residual resistivity caused by GBs. However, it should be mentioned that it is the field-induced downshift of T_p that also results in the suppression of resistivity and hence the enhancement of MR near room temperature.

Fig. 8 presents MR ratio as a function of applied field for $(LCMO)_{1-x}Ag_x$. We can find the low-field MR at 5 K is reduced with increasing Ag content, which can be explained in the model of spin-polarized electron tunneling. New conduction channels blocked at GBs will be opened due to the connection through the Ag grains, in other words, Ag addition is equivalent to the reduction of GBs proportion in LCMO system, thus accordingly the tunneling effect will be reduced. Nevertheless, MR at 300 K is larger for $x = 0.10$ than for $x = 0.05$, reporting that increasing Ag content favors room-temperature MR.

As depicted by Shreekala et al. [10], the improvement of morphology is also important to the changes in magnetic/transport properties. As shown in Figs. 3 and 4, LCMO grains become perfect and uniform. This is due to the catalytic effect of Ag during the perovskite formation. Because LCMO grain sizes are not changed with different Ag content, we need not consider the grain size effects. First, enhanced T_C demonstrates that well crystallization and uniform of LCMO grains are very important to the T_C enhancement. We suggest that well crystallization and uniform of LCMO give rise to the suppression of magnetic scattering at GBs. Secondly, metallic conduction channels penetrated into the insulating regions can remarkably elevate the T_p and lower the resistivity, whereas the well crystallization at GBs brings about another contribution to T_p enhancement and ρ reduction.

4. Conclusions

Interesting phenomena are observed in the present granular Ag-added LCMO, including the pronounced enhancements in T_C, T_p and MR near room temperature, dramatic reduction in resistivity, downshifts in upturn of low-temperature resistivity and field-induced M–I transition. The XRD patterns and TGA–DTA runs have revealed the existence of segregated metal silver. By connection through the silver grains, a new electron transport channel blocked at GBs of LCMO is opened, enhancing the GB conductivity. In addition, both SEM and HRTEM images show that Ag addition makes the LCMO crystallites become more perfect and uniform, suppressing the magnetic scattering at GBs. This should be the main reason for the T_C enhancement. Metallic conduction channels penetrated into the insulating regions can remarkably elevate the T_p and lower the resistivity, whereas the well crystallization at GBs brings about another contribution to T_p enhancement and ρ reduction. The observations are profitable for us to recognize the promising applications of the metal-introduced manganites.

Acknowledgments

The authors acknowledge the support of MOST of China (G19980613), NSFC (Nos. 50272006, 20221101 & 20023005), Training Project for Doctoral Student of MOE, and Founder Foundation of PKU.

References

[1] P. Schiffer, A.P. Ramirez, W. Bao, S.W. Cheong, Phys. Rev. Lett. 75 (1995) 3336.
[2] R. Mahendiran, S.K. Tiwary, A.K. Raychaudhuri, T.V. Ramakrishnan, R. Mahesh, N. Rangavittal, C.N.R. Rao, Phys. Rev. B 53 (1996) 3348.
[3] S.B. Oseroff, M. Torikachvili, J. Singley, S. Ali, S.W. Cheong, S. Schultz, Phys. Rev. B 53 (1996) 6521.
[4] C.H. Booth, F. Bridges, G.H. Kwei, J.M. Lawrence, A.L. Cornelius, J.J. Neumeier, Phys. Rev. Lett. 80 (1998) 853.
[5] B. Raveau, A. Maignan, C. Martin, M. Hervieu, Chem. Mater. 10 (1998) 2641.
[6] C. Zener, Phys. Rev. 82 (1951) 403.
[7] R. Shreekala, M. Rajeswari, R.C. Srivastava, K. Ghosh, A. Goyal, V.V. Srinivasu, S.E. Lofland, S.M. Bhagat, M. Downes, R.P. Sharma, S.B. Ogale, R.L. Greene, R. Ramesh, T. Venkatesan, R.A. Rao, C.B. Eom, Appl. Phys. Lett. 74 (1999) 1886.
[8] A.K. Pradhan, B.K. Roul, J.G. Wen, Z.F. Ren, M. Muralidhar, P. Dutta, D.R. Sahu, S. Mohanty, P.K. Patro, Appl. Phys. Lett. 76 (2000) 763.
[9] A.K. Pradhan, B.K. Roul, Y. Feng, Y. Wu, S. Mohanty, D.R. Sahu, P. Dutta, Appl. Phys. Lett. 78 (2001) 1598.
[10] R. Shreekala, M. Rajeswari, S.P. Pai, S.E. Lofland, V. Smolyaninova, K. Ghosh, S.B. Ogale, S.M. Bhagat, M.J. Downes, R.L. Greene, R. Ramesh, T. Venkatesan, Appl. Phys. Lett. 74 (1999) 2857.

[11] R. Bathe, K.P. Adhi, S.I. Patil, G. Marest, B. Hannoyer, S.B. Ogale, Appl. Phys. Lett. 76 (2000) 2104.
[12] N. Khare, U.P. Moharil, A.K. Gupta, H.K. Singh, O.N. Srivastava, J. Appl. Phys. 89 (2001) 3532.
[13] J. Li, Q. Huang, Z.W. Li, L.P. You, S.Y. Xu, C.K. Ong, J. Appl. Phys. 89 (2001) 7428.
[14] Y.H. Huang, C.H. Yan, F. Luo, W. Song, Z.M. Wang, C.S. Liao, Appl. Phys. Lett. 81 (2002) 76.
[15] H.Y. Hwang, S.W. Cheong, N.P. Ong, B. Batlogg, Phys. Rev. Lett. 77 (1996) 2041.
[16] R. Mahesh, R. Mahendiran, A.K. Raychaudhuri, C.N.R. Rao, Appl. Phys. Lett. 68 (1996) 2291.
[17] Y.H. Huang, Z.G. Xu, C.H. Yan, Z.M. Wang, T. Zhu, C.S. Liao, S. Gao, G.X. Xu, Solid State Commun. 114 (2000) 43.
[18] P.A. Joy, S.K. Date, Appl. Phys. Lett. 76 (2000) 1209.
[19] T. Tang, Q.Q. Cao, K.M. Gu, H.Y. Xu, S.Y. Zhang, Y.W. Du, Appl. Phys. Lett. 77 (2000) 723.
[20] A. de Andrés, M. García-Hernández, J.L. Martínez, Phys. Rev. B 60 (1999) 7328.
[21] S. Pignard, H. Vincent, J.P. Senateur, K. Frohlich, J.I. Souc, Appl. Phys. Lett. 73 (1998) 999.
[22] Ll. Balcells, B. Martínez, F. Sandiumenge, J. Fontcuberta, J. Magn. Magn. Mater. 211 (2000) 193.